THE ASTROPHYSICAL JOURNAL, 442:259–272, 1995 March 20

GRAVITATIONAL RADIATION FROM RAPIDLY ROTATING NASCENT NEUTRON STARS

DONG LAI[1] AND STUART L. SHAPIRO[2]
Center for Radiophysics and Space Research, Cornell University, Ithaca, NY 14853
Received 1994 May 31; accepted 1994 September 28

ABSTRACT

We study the secular evolution and gravitational wave signature of a newly formed, rapidly rotating neutron star. The neutron star may arise from core collapse in a massive star or from the accretion-induced collapse of a white dwarf. After a brief dynamical phase, the nascent neutron star settles into an axisymmetric, secularly unstable equilibrium state. Gravitational radiation drives the star to a nonaxisymmetric, stationary equilibrium configuration via the bar-mode instability. The emitted quasi-periodic gravitational waves have a unique signature: the wave frequency sweeps downward from a few hundred Hertz to zero, while the wave amplitude increases from zero to a maximum and then decays back to zero. Such a wave signal could be detected by broadband gravitational wave interferometers currently being constructed.

We also characterize two other types of gravitational wave signals that could arise in principle from a rapidly rotating, secularly unstable neutron star: a high-frequency ($f \gtrsim 1000$ Hz) wave which increases the pattern-speed of the star, and a wave that actually increases the angular momentum of the star.

Subject headings: hydrodynamics — instabilities — radiation mechanisms: nonthermal — stars: neutron — supernovae: general

1. INTRODUCTION

The advent of the new generation of gravitational wave detectors, such as the Laser Interferometer Gravitational Wave Observatory (LIGO; see Abramovici et al. 1992) and its French-Italian counterpart VIRGO (Bradaschia et al. 1990), stimulates a renewed interest in astrophysical sources of gravitational waves (Thorne 1987, 1992). Of special importance are those sources that radiate in LIGO's sensitivity band, 10–1000 Hz. In this paper we study possible unique gravitational wave signals with frequency in this range from newly formed neutron stars.

Gravitational collapse leading to the formation of a neutron star has long been considered an observable source of gravitational radiation. The event rate of type II supernovae is estimated to be several per year out to a distance of 10 Mpc, the distance to the Virgo cluster of galaxies (van den Bergh & Tammann 1991). The rate of electromagnetically "quiet" gravitational collapses (such as accretion-induced collapse of white dwarfs) may be as high as one per galaxy every 1 to 5 years (Bahcall & Piran 1983; Blair 1989). However, the strengths of gravitational wave signals from core collapse are still highly uncertain because they depend crucially on the unknown asymmetry of the collapse. If the collapse is axisymmetric, the energy radiated during the implosion phase of the collapse is at most $\sim 5 \times 10^{-8}\, Mc^2$ (Finn 1991; Mönchmeyer et al. 1991). Such a supernova would not be detectable, even by the advanced LIGO detectors, for sources beyond our Galaxy and the Magellanic clouds. However, it is widely expected that if the collapsing and bouncing core rotates so rapidly that it becomes nonaxisymmetric, the efficiency of producing gravitational wave can be much higher. So far, nonaxisymmetric core collapse has only been studied based on classical homogeneous ellipsoid models (see Saenz & Shapiro 1981 and references therein) and three-dimensional numerical calculations of the prebounce phase of the collapse has been performed by Bonazzola & Marck (1993).

It is well known that nonaxisymmetric instabilities can develop in rapidly rotating fluid bodies when the ratio $\beta \equiv T/|W|$ of the rotational energy T to the gravitational potential energy W is sufficiently large (Chandrasekhar 1969; hereafter referred as Ch69). A star becomes dynamically unstable when $\beta > \beta_{\rm dyn} \simeq 0.27$, while its $l = m = 2$ "bar" mode oscillations become secularly unstable due to viscosity (Roberts & Stewartson 1963) or gravitational radiation reaction (Chandrasekhar 1970a) when $\beta > \beta_{\rm sec} \simeq 0.14$. The gravitational radiation (GR) instability for higher-order modes ($m > 2$) can set in at even smaller value of β (Friedman & Schutz 1978, Comins 1979a, b). When the degenerate core of a massive star or when a white dwarf with mass exceeding the Chandrasekhar limit collapses to form a neutron star, the value of β can increase significantly. Assuming angular momentum conservation, the collapsed star would have

$$\frac{T}{|W|} = \frac{R_i}{R}\left(\frac{T}{|W|}\right)_i,$$

where R_i and R are the radius of the core before and after collapse, and β_i refers to the precollapse initial value. Typically, $R_i \sim 1500$ km for a white dwarf near the Chandrasekhar mass, and $R \sim 10$ km for a neutron star; hence $R_i/R \sim 10^2$. Thus the nascent neutron star can be rapidly rotating even if the initial precollapse core is not.

While there are no direct observations of the rotation of precollapse cores—they are hidden inside the envelopes of giant stars—the situation for the accretion-induced collapse of white dwarf and for the collapse of merging white dwarf binaries may be clearer. In both cases, the precollapse white dwarfs can attain sufficient angular momentum from the accreting gas or from the initial binary orbits. Although most millisecond pulsars are thought to have been spun up by accretion, it has been suggested that some millisecond pulsars originate from the collapse of white dwarfs in binary systems

[1] Current address: Theoretical Astrophysics 130–33, California Institute of Technology, Pasadena, CA 91125; dong@tapir.caltech.edu.
[2] Department of Astronomy and Physics, Cornell University; shapiro@astrosun.tn.cornell.edu.

(Michel 1987; van den Heuvel 1987; Bailyn & Grindlay 1990). The initial spins of ordinary radio pulsars are not well constrained by the pulsar statistics; but it is possible that some radio pulsars are created with high initial spin. Although the physical mechanism that gives rise to the high velocity (~ 1000 km s^{-1}) of some radio pulsars such as PSR 2224+65 (Cordes, Romani, & Lundgren 1993) is not completely clear (see Radhakrishnan 1992 for a review), it is conceivable that rapid rotation and asymmetry of the collapsed core play an important role. Finally, there may already be some indirect observational evidence for asymmetric core collapse: the spectropolarimetry of SN 1987a (Cropper et al. 1988) and SN 1993J (Trammell, Hines, & Wheeler 1993), as well as emission-line profiles in the spectra of SN 1993J (Spyromilio 1994), indicate an asymmetric atmosphere in both supernovae.

A new-born neutron star can be secularly unstable but dynamically stable ($\beta_{\rm sec} < \beta < \beta_{\rm dyn}$) only if the rotation rate of the precollapse core lies in a narrow range. Thus it is more likely that the core becomes dynamically unstable ($\beta > \beta_{\rm dyn}$) following collapse, provided that the initial β_i is not too small. The fate of a dynamically unstable rotating star has been studied numerically by Durisen et al. (1986), Williams & Tohline (1988), and more recently by Houser, Centrella, & Smith (1994), who have also calculated the resulting gravitational waves due to the dynamical instability. According to Houser et al. (1994), the instability develops as follows: after shedding mass and angular momentum in the form of two tailing spiral arms, which then expand and merge, causing shock dissipation, the system evolves on a dynamical timescale toward a nearly axisymmetric equilibrium state. Its β falls below the dynamical stability limit $\beta_{\rm dyn}$, but remains much larger than the secular stability limit $\beta_{\rm sec}$. Such a postcollapse, axisymmetric core will evolve into a nonaxisymmetric configuration on a secular dissipation timescale. The main purpose of our paper is to study the growth of this secular instability (§ 2) and to characterize the resulting gravitational wave form (§ 3). We follow the secular evolution using a compressible ellipsoid model, which we have recently developed to study the equilibrium and dynamics of rotating stars and binary systems (Lai, Rasio, & Shapiro 1993, 1994, hereafter referred as Paper I and Paper II). We shall see that for the typical neutron star with mass $M \sim 1.4\ M_\odot$ and radius $R \sim 10$ km, the gravitational wave amplitude increases from zero to a maximum and then decreases to zero again, while the wave frequency sweeps from a few hundred Hertz down to zero (see Fig. 4 below). Such a gravitational wave signal can in principle be detected by LIGO (§ 3.3, especially Fig. 6).

Another purpose of our paper is to characterize *all* types of gravitational waveforms one can expect from a rotating star modeled as a compressible fluid ellipsoid. The secular evolution of homogeneous, incompressible ellipsoidal figures has been studied before (Miller 1974; Detweiler & Lindblom 1977), but the waveforms have not been considered or characterized. In addition to the low-frequency wave considered in § 3, we find two other types of wave forms: a high-frequency wave with decreasing amplitude and increasing frequency, and a peculiar wave which increases the angular momentum of the star. These are discussed in § 4.

The fluid viscosity can have some effects on the secular instability and the evolution. These effects are discussed in § 5. A summary including a discussion of the main uncertainties is given in § 6.

We use units such that $G = c = 1$ throughout the paper.

2. GRAVITATIONAL RADIATION INSTABILITY IN ROTATING STARS

Chandrasekhar (1970a) first discovered that the GR reaction can induce a nonaxisymmetric secular instability in a uniformly rotating, incompressible Maclaurin spheroid. He found that the $l = m = 2$ "bar" mode (with angular behavior of the form $e^{\pm im\phi}$) becomes unstable beyond the point at which the nonaxisymmetric Jacobi sequence or Dedekind sequence bifurcates from the axisymmetric Maclaurin sequence (Ch69). At the bifurcation point, the ratio of the kinetic energy and the absolute value of the potential energy $\beta \equiv T/|W|$ equals $\beta_{\rm sec} = 0.1375$.

We have reanalyzed this bar-mode instability induced by GR as well as by viscosity in *compressible* rotating stars (Appendix A). Our analysis is based on the equilibrium and dynamical ellipsoid model developed in Papers I–II, in which a rotating star is treated as a self-similar ellipsoid with polytropic density and linear velocity profiles. We have extended many known results concerning incompressible ellipsoidal figures (Ch69) to their compressible analogs. In particular, we find that, just as in the incompressible case, the secular instability sets in at the bifurcation point, where $\beta = \beta_{\rm sec} = 0.1375$ independent of the polytropic index n. Similarly, a dynamical bar-mode instability sets in at $\beta = \beta_{\rm dyn} = 0.2738$. While for strictly uniformly rotating stars, mass-shedding can occur before the point of bifurcation for $n > 0.808$ (James 1964; see Tassoul 1978 for review), a slight amount of differential rotation can in principle inhibit mass shedding without changing the global structure of the star. Indeed, axisymmetric models of differentially rotating polytropes which retain the global properties of Maclaurin spheroids have been constructed by Bodenheimer & Ostriker (1973). Our finding that the secular and dynamical stability limits do not depend sensitively on the polytropic index n as well as differential rotation law is also corroborated by earlier numerical studies (Ostriker & Bodenheimer 1973; see also Managan 1985; Imamura, Friedman, & Durisen 1985; Ipser & Lindblom 1990).

Along an equilibrium Maclaurin sequence parameterized by the eccentricity e, the ratio β and the dimensionless angular velocity $\hat{\Omega}_M$ are given by

$$\beta = \frac{3}{2e^2}\left[1 - \frac{e(1-e^2)^{1/2}}{\sin^{-1} e}\right] - 1\ , \tag{2.1}$$

$$\hat{\Omega}_M^2 \equiv q_n \frac{\Omega_M^2}{\pi\bar{\rho}} = 2\left[\frac{(1-e^2)^{1/2}}{e^3}(3-2e^2)\sin^{-1} e - \frac{3(1-e^2)}{e^2}\right], \tag{2.2}$$

where $q_n = (1 - n/5)\kappa_n$, $\kappa_n \leq 1$ is a constant of order unity which depends only on n (see Table I in Paper I), and $\bar{\rho} = 3M/(4\pi R^3)$ is the mean density. Equations (2.1)–(2.2) are the same as the expressions for incompressible Maclaurin spheroids (Ch69), but they are also valid for compressible configurations within our approximation. Because of the centrifugal support, the size of the star increases as the rotation rate increases. The mean radius of the rotating star $R \equiv (a_1 a_2 a_3)^{1/3}$ is given by

$$R = R_0\left[\frac{\sin^{-1} e}{e}(1-e^2)^{1/6}(1-\beta)\right]^{-n/(3-n)}\ , \tag{2.3}$$

where R_0 is the radius of the nonrotating star with the same mass. For a given equation of state and mass, R_0 is uniquely

determined. In a rotating frame with angular frequency Ω, our analysis (Appendix A) yields the bar-mode frequency

$$\sigma_{\pm}(\Omega) = (2\Omega - \Omega_M) \pm \sigma_0 , \tag{2.4}$$

where

$$\sigma_0 = \left(\frac{4}{q_n}\pi\bar{\rho}B_{11} - \Omega_M^2\right)^{1/2} , \tag{2.5}$$

and B_{11} is the index symbol as defined in Ch69 (chap. 3), and depends only on the axis ratios. Gravitational radiation destabilizes the Dedekind-mode (the mode with plus sign in eq. [2.4]) when $\hat{\Omega}_M^2 > 2B_{11}$, or equivalently, when $\beta > \beta_{\rm sec}$. The growth time $\tau_{\rm GW}$ for the secular instability is given by

$$\tau_{\rm GW} = \frac{25}{2\kappa_n M a_1^2}\frac{\sigma_0}{(\Omega_M - \sigma_0)^5} = 0.084 M_{1.4}^{-3} R_{10}^4 \kappa_n \left(1 - \frac{n}{5}\right)^2 \times \left[\left(\frac{R}{R_0}\right)^4 \frac{(1-e^2)^{1/3}\hat{\sigma}_0}{(\hat{\Omega}_M - \hat{\sigma}_0)^5}\right] \text{s} , \tag{2.6}$$

where $M_{1.4} \equiv M/(1.4\ M_\odot)$, $R_{10} \equiv R_0/(10\ \text{km})$, and $\hat{\sigma}_0 \equiv q_n^{1/2}\sigma_0/(\pi G\bar{\rho})^{1/2} = (4B_{11} - \hat{\Omega}_M^2)^{1/2}$ (eq. [2.5]). For $0 < \beta - \beta_{\rm sec} \ll 1$, equation (2.6) can be approximately written as

$$\tau_{\rm GW} \simeq 2 \times 10^{-5} M_{1.4}^{-3} R_{10}^4 (\beta - \beta_{\rm sec})^{-5} \text{ s} , \tag{2.7}$$

Figure 1 shows the $\tau_{\rm GW}$ as a function of $\beta = T/|W|$ for $n = 0$, 0.5, 1. We see that for large β, the growth time $\tau_{\rm GW}$ is larger for more compressible stars because of the rotation-induced expansion of the star (eq. [2.3]). However, for $n \sim 0.5$–1, typical of neutron stars, $\tau_{\rm GW}$ does not depend sensitively on the polytropic index n. Thus for a neutron star with $M = 1.4\ M_\odot$, $R_0 = 10$ km, we have $\tau_{\rm GW} \simeq 7 \times 10^4$ s for $\beta = 0.15$, $\tau_{\rm GW} \simeq 20$ s for $\beta = 0.20$, and $\tau_{\rm GW} \simeq 1$ s for $\beta = 0.24$.

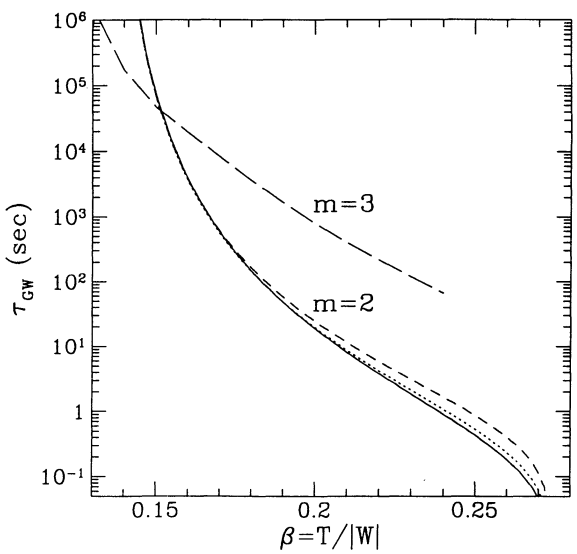

FIG. 1.—The secular instability growth time due to gravitational radiation as a function of the ratio $\beta = T/|W|$ for a neutron star modeled as a compressible Maclaurin spheroid, with $M = 1.4\ M_\odot$ and $R_0 = 10$ km. The solid line corresponds to the bar-mode ($m = 2$) instability for polytropic index $n = 0$, the dotted line for $n = 0.5$, and the short-dashed line for $n = 1$. The long-dashed line is for the $m = 3$ mode and $n = 0$.

Higher order ($m > 2$) modes can become unstable at a smaller β. In fact, gravitational radiation tends to make all rotating stars unstable (Friedman & Schutz 1978). However, the growth time of this gravitational radiation instability increases rapidly as m increases (Comins 1979a, b). Moreover, viscosity tends to counteract this instability (Lindblom & Detweiler 1977), and the stabilizing effect becomes more efficient for higher order modes. Thus we will not discuss these high-order instabilities for $\beta > \beta_{\rm sec}$; the consequences of these instabilities are not as clear as that of the bar-mode instability. Note that for β just slightly larger than $\beta_{\rm sec}$, the growth time for the $m = 2$ mode instability is longer than that of a $m > 2$ mode (as seen in Fig. 1, where the result for the $m = 3$ mode is from Comins 1979b, for $n = 0$). Thus our discussion below about the evolution will not be applicable to those very small values of $\beta - \beta_{\rm sec}$. However, for $\beta > 0.17$, the growth time for the bar-mode is much shorter (by more than a factor of 10) than that of the $m = 3$ mode. Therefore, for these values of β, the bar-mode instability is much stronger than the higher-order modes, and our discussion of the secular evolution is valid.

Note that we have normalized the mass and radius to those of a cold, nonrotating neutron star. Following its implosion, which takes ~ 1 s, the 1.4 $M_\odot$ collapsing core settles into hydrostatic equilibrium within a few milliseconds. This hot protoneutron star does not resemble a usual cold neutron star, as it consists of an unshocked cold inner core with radius ~ 10 km surrounded by a shocked hot outer core (mantle) which extends to ~ 100 km. The protoneutron star evolves quasi-statically via neutrino cooling. However, within one second, the outer mantle cools and contracts significantly, and the protoneutron star (with mass $\sim 1.4\ M_\odot$) approaches a canonical radius of 10 km. By this time, the hydrostatic structure of the neutron star more or less resembles that of a cold neutron star, although the star will remain very hot ($T \gtrsim 10^{10}$ K) for more than a few tens of seconds (Burrows & Lattimer 1986; Burrows 1990). Since the nonaxisymmetric instability growth time is typically larger than a second, it is appropriate to use the canonical radius of a cold neutron star (but see § 6).

3. EVOLUTION AND GRAVITATIONAL WAVEFORM

Here we discuss the evolution of a rotating star modeled as a nonaxisymmetric ellipsoid (i.e., a Riemann-S ellipsoid in the language of Ch69 and Paper I) under the influence of gravitational radiation reaction and zero viscosity.

3.1. *Secular Evolution*

A secularly unstable Maclaurin spheroid will evolve away from the axisymmetric configuration due to gravitational radiation. The evolution can in principle be studied using the full dynamical equations of ellipsoidal figures (Ch69; Miller 1974; Paper II) including gravitational radiation reaction. However, since the growth time of the instability $\tau_{\rm GW}$ is generally much longer than the dynamical time of the star, the evolution is quasi-static, i.e., the star will evolve along an equilibrium sequence of Riemann-S ellipsoids (Ch69, Paper I). A general Riemann-S ellipsoid is characterized by the angular velocity $\boldsymbol{\Omega} = \Omega \boldsymbol{e}_z$ *of the ellipsoidal figure* (the pattern speed) about a principal axis and the internal motion of the fluid with uniform vorticity $\boldsymbol{\zeta} = \zeta \boldsymbol{e}_z$ along the same axis (in the frame corotating with the figure). The vorticity in the inertial frame is then $\boldsymbol{\zeta}^{(0)} = 2\boldsymbol{\Omega} + \boldsymbol{\zeta}$. Since the gravitational radiation reaction acts like a potential force, the fluid circulation C along the equator

of the star is conserved in the absence of viscosity (Miller 1974; Paper II). Following Paper I (§ 5.1) we write

$$\mathscr{C} \equiv \left(-\frac{1}{5\pi}\kappa_n M\right) C = \left(-\frac{1}{5\pi}\kappa_n M\right) \times \pi a_1 a_2 \zeta^{(0)} = I\Lambda - \frac{2}{5}\kappa_n M a_1 a_2 \Omega\,, \tag{3.1}$$

where $I = \kappa_n M(a_1^2 + a_2^2)/5$ is the moment of inertia, and $\Lambda = -a_1 a_2 \zeta/(a_1^2 + a_2^2)$. The quantity $\mathscr{C}$ has the dimension of angular momentum but is proportional to the conserved circulation $C \equiv \pi a_1 a_2 \zeta^{(0)}$. We refer to $\mathscr{C}$ itself as the circulation for convenience. Note that in the same notation, the angular momentum of the ellipsoid is

$$J = I\Omega - \tfrac{2}{5}\kappa_n M a_1 a_2 \Lambda\,. \tag{3.2}$$

Thus, under the influence of gravitational radiation reaction, and when the viscous dissipation is negligible, a secularly unstable Maclaurin spheroid will evolve along a constant-$\mathscr{C}$ equilibrium sequence, and proceed ultimately toward a Dedekind ellipsoid, for which $\Omega = 0$ (a "stationary football"). The evolution track can be best illustrated by the diagram shown in Figure 2, which depicts the equilibrium energies for various constant $-\mathscr{C}$ sequences as functions of the axis ratio a_2/a_1, all for $n = 1$. For comparison, the Jacobi and the Dedekind sequences are also shown, while the Maclaurin sequence corresponds to the vertical line with $a_2/a_1 = 1$. A given Maclaurin spheroid has a unique value of $\mathscr{C}$, but two different constant $-\mathscr{C}$ sequences branch off: one sequence is *Jacobi-like*, with $|\zeta| < 2|\Omega|$, the other is *Dedekind-like*, with $|\zeta| > 2|\Omega|$. Clearly, the endpoint of the evolution depends on the value $|\mathscr{C}|$ of the initial configuration. For $|\mathscr{C}| < |\mathscr{C}_{\rm sec}|$, where $\mathscr{C}_{\rm sec}$ is the circulation of a Maclaurin spheroid at the bifurcation point, the Maclaurin spheroid is the lowest energy terminal state toward which both Jacobi-like and Dedekind-like configurations evolve; for $|\mathscr{C}| > |\mathscr{C}_{\rm sec}|$, on the other hand, the terminal state is a Dedekind ellipsoid. A Jacobi-like configuration with $|\mathscr{C}| > |\mathscr{C}_{\rm sec}|$ first evolves toward an axisymmetric, Maclaurin state, and then continues through a Dedekind-like phase toward a Dedekind ellipsoid. The value of $|\mathscr{C}_{\rm sec}| = J_{\rm sec}$ is given by

$$J_{\rm sec} = 0.304\left(\frac{\kappa_n}{1 - n/5}\right)^{1/2} (M^3 R)^{1/2}\,, \tag{3.3}$$

(see eq. [3.27] and Table II in Paper I), where R is given by equation (2.3).

Now let us focus on the evolution of a secularly unstable Maclaurin spheroid toward a Dedekind ellipsoid, corresponding to region I in Figure 2. The initial Maclaurin spheroid has angular momentum $J_i = |\mathscr{C}_i|$. The final Dedekind state has $J_f = |\mathscr{C}_i|[2a_1 a_2/(a_1^2 + a_2^2)]_f$ (cf. eqs. [3.1]–[3.2] with $\Omega = 0$), the total angular momentum radiated in gravitational wave is given by

$$\Delta J = J_i\left[\frac{(a_1 - a_2)^2}{a_1^2 + a_2^2}\right]_f\,, \tag{3.4}$$

where the subscript "f" stands for the final Dedekind configuration. The total energy ΔE emitted as gravitational wave for a secularly unstable Maclaurin spheroid can be calculated by comparing the difference in equilibrium energy between the Maclaurin spheroid and the Dedekind ellipsoid with the same $\mathscr{C}$. Figure 3 shows the dependence of ΔE as a function of $\beta = T/|W|$ of the initial Maclaurin spheroid. We see that ΔE does not depend sensitively on the compressibility for $n \lesssim 1$. Thus the energy radiated in gravitational wave during the Maclaurin-Dedekind transition can be as large as $0.02M^2/R_0$, or $\Delta E \lesssim 4 \times 10^{-3}\ M$ for a typical neutron star radius

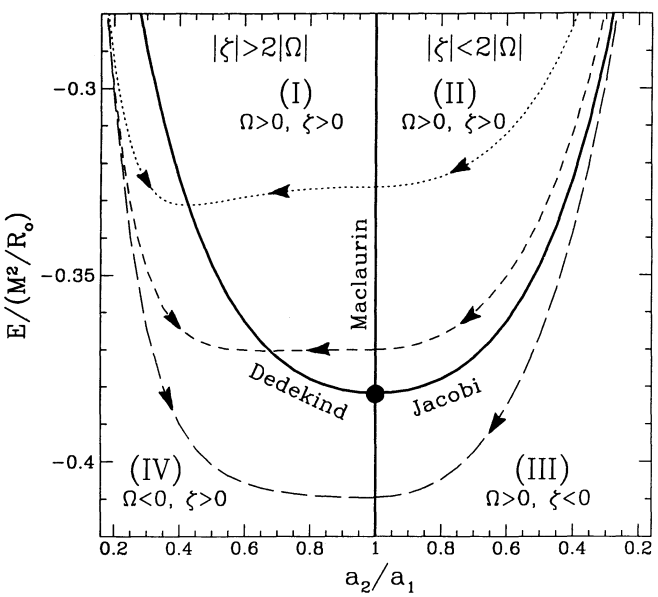

FIG. 2.—Secular evolution tracks of a Riemann-S ellipsoid with $n = 1$ driven by gravitational radiation reaction. The energy of an ellipsoid as a function of the axis ratio a_2/a_1 is shown along various equilibrium sequences. Dedekind-like sequences ($|\zeta| > 2|\Omega|$) are shown on the left panel, Jacobi-like ($|\zeta| > 2|\Omega|$) on the right panel. The thick solid curves correspond to the Dedekind and Jacobi sequences, the thick vertical line corresponds to the Maclaurin sequence, while the other lines correspond to constant-$\mathscr{C}$ sequences: $\bar{\mathscr{C}} = \mathscr{C}/(M^3 R_0)^{1/2} = -0.4$ (*dotted line*), $\bar{\mathscr{C}} = -0.32$ (*dashed line*), and $\bar{\mathscr{C}} = -0.25$ (*long-dashed line*). The solid round dot marks the point of bifurcation. The Dedekind-like panel is divided into region *I* ($\Omega > 0$, $\zeta > 0$) and region IV ($\Omega < 0$, $\zeta > 0$) by the Dedekind line (*solid curve*), while the Jacobi-like panel is divided by the Jacobi line into region II ($\Omega > 0$, $\zeta > 0$) and region III ($\Omega > 0$, $\zeta < 0$).

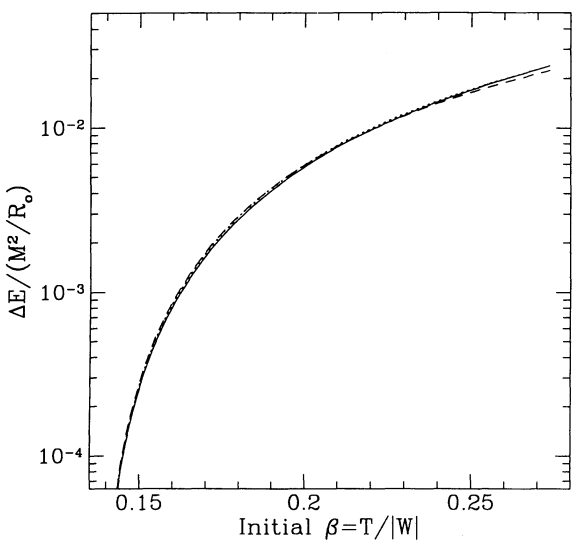

FIG. 3.—The total energy radiated in gravitational wave during the evolution of a star from a Maclaurin spheroid to a Dedekind ellipsoid as a function of the initial $T/|W|$. The solid line is for $n = 0$, the dotted line for $n = 0.5$, and the dashed line for $n = 1$.

($R_0/M \simeq 5$). This is much larger than the energy radiated ($\lesssim 5 \times 10^{-8}\ M$) in an axisymmetric collapse preceding the neutron star formation (Finn 1991; Mönchmeyer et al. 1991).

3.2. *Gravitational Wave Amplitude*

The gravitational wave emitted during the Maclaurin-Dedekind evolution has certain unique characteristics. At the beginning of the evolution, the wave amplitude is small since the star is still nearly axisymmetric. Near the end of the evolution, as the star approaches a Dedekind configuration asymptotically, the wave amplitude is small again because the angular velocity Ω of the figure becomes decreasingly small. Thus we expect *a nonmonotonic behavior of the gravitational wave amplitude during such an evolution, while the wave frequency decreases monotonically.*

In the weak-field, slow-motion limit, the gravitational radiation can be calculated by the standard quadrupole formula (see, e.g., Misner, Thorne, & Wheeler 1970). The rates of energy loss and angular momentum loss are given by

$$\left(\frac{dE}{dt}\right)_{\rm GW} = \Omega\left(\frac{dJ}{dt}\right)_{\rm GW} = -\frac{32}{5}\,\Omega^6(I_{11}-I_{22})^2\,, \qquad (3.5)$$

where $I_{ii} = \kappa_n M a_i^2/5$ are the components of the star's quadrupole moment along the principal axes in its equatorial plane. At a distance D from the source, the two polarization components of the waveforms are

$$h_+ = -\frac{2}{D}\,\Omega^2(I_{11}-I_{22})\cos\Phi(1+\cos^2\theta)\,,$$
$$h_\times = -\frac{4}{D}\,\Omega^2(I_{11}-I_{22})\sin\Phi\cos\theta\,, \qquad (3.6)$$

where θ is the angle between the rotation axis of the star and line of sight from the earth, and $\Phi \equiv 2\int^t \Omega\,dt$ is twice the orbital phase. The wave is quasi-periodic, with frequency $f = \Omega/\pi$ and amplitude (for $\theta = 0$)

$$h = \frac{4}{D}\,\Omega^2(I_{11}-I_{22})\,. \qquad (3.7)$$

Typical wave amplitudes as a function of frequency are shown in Figure 4, for polytropic index $n = 0.5$ and 1. The initial Maclaurin spheroids have $\beta = 0.2$ and $\beta = 0.24$, respectively. The wave sweeps with time from high frequency to low, that is, from right to left in Figure 4. Also shown in the figure are the timescale of the evolution as measured by $|dt/d\ln f| = |f/\dot{f}|$, and the number of cycles gravitational wave spent near frequency f

$$\left|\frac{dN}{d\ln f}\right| = \left|\frac{f^2}{\dot{f}}\right| = \frac{\Omega^2}{\pi}\left|\frac{dE}{d\Omega}\right|_{\rm eq}\left|\left(\frac{dE}{dt}\right)^{-1}_{\rm GW}\right|, \qquad (3.8)$$

where $dE/d\Omega$ is evaluated along an equilibrium sequence with constant $\mathscr{C}$. The number of cycles near the frequency at which the wave amplitude is maximum depends sensitively on the initial value of β, and to a less extent, on the polytropic index. But even for the initial β close to the dynamical limit $\beta_{\rm dyn}$, there are still $\gtrsim 10^3$ cycles when the wave amplitude is close to the maximum. Note that at the beginning of the evolution ($f \to f_{\rm max}$), the timescale approaches infinity. This is because we have assumed exact equilibrium models, and a *perfect* Maclaurin spheroid does not evolve at all. In reality, a small perturbation will make the Maclaurin spheroid evolve on the order of a few growth time $\tau_{\rm GW}$, as determined in § 2. This time is of the same order of magnitude as the time the system spends near the maximum amplitude phase.

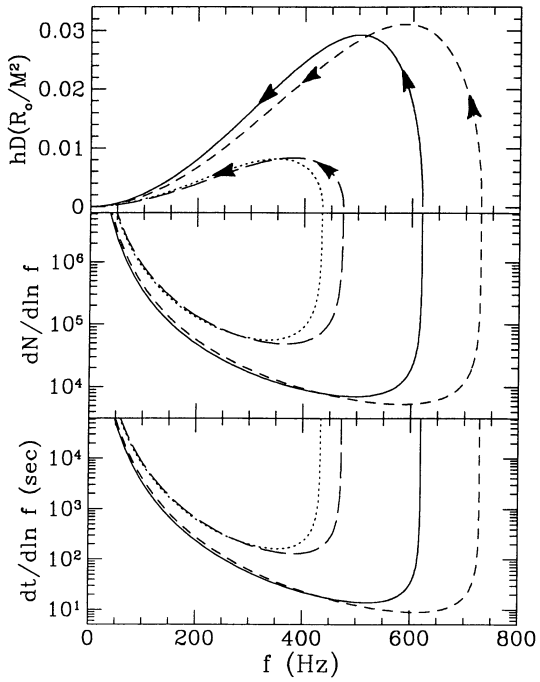

FIG. 4.—The gravitational waves emitted by a secularly unstable neutron star, evolving from a Maclaurin spheroid toward a Dedekind ellipsoid. (*top*) shows the gravitational wave amplitude as a function of frequency; (*middle*) the number of cycles spent near f, and (*bottom*) the timescale of the evolution. Here $M = 1.4M_\odot$, $R_0 = 10$ km and D is the distance to the star. The solid lines correspond to the initial $\beta = 0.24$ and the dotted lines $\beta = 0.2$, both for $n = 1$; the dashed lines correspond to $\beta = 0.24$ and the long-dashed lines $\beta = 0.2$, both for $n = 0.5$.

It is important to note that *the wave frequency is determined by the pattern speed Ω of the ellipsoidal figure, and this frequency can be much lower than the rotational frequency of the secularly unstable star.* During the evolution, the wave frequency decreases monotonically from an initial value to zero. Consider the maximum frequency of the wave, corresponding to the frequency near the beginning of the evolution, when the star is still close to a Maclaurin spheroid. The bar-mode oscillation frequency as viewed in a general rotating frame is given by equation (2.4), and gravitational radiation destabilizes the Dedekind mode. In a particular reference frame, with angular velocity $\Omega_{\rm max}$, the Dedekind-mode can be neutralized, i.e., $\sigma_+(\Omega_{\rm max}) = 0$. It is along the axes of this rotating frame that the Maclaurin spheroid starts deforming into a nonaxisymmetric shape. Therefore, as the Maclaurin spheroid begins to evolve due to gravitational radiation, the pattern speed $\Omega_{\rm max}$ is given by

$$\Omega_{\rm max} = \tfrac{1}{2}(\Omega_M - \sigma_0)\,, \qquad (3.9)$$

which is always smaller than the initial rotation rate Ω_M of the star. Clearly, at the bifurcation point, $\Omega_{\rm max} = 0$ (i.e., at the bifurcation point, the oscillation mode is neutralized in the inertial frame). The angular frequency $\Omega_{\rm max}$ is also one of the two values assigned to a Maclaurin spheroid if it is to be considered as a limiting member of Riemann ellipsoids (Ch69,

§ 48). Equation (3.9) is simply half of the absolute value of the mode frequency $\sigma_+(0)$ in the inertial frame. The maximum frequency of the gravitational wave during the Maclaurin-Dedekind evolution is then

$$f_{\max} = \frac{\Omega_{\max}}{\pi} = \frac{\sqrt{3}}{4\pi}\left(\frac{GM}{R_0^3}\right)^{1/2} q_n^{-1/2}\left(\frac{R_0}{R}\right)^{3/2}(\hat{\Omega}_M - \hat{\sigma}_0)$$

$$= 1.88 \times 10^3\, M_{1.4}^{1/2} R_{10}^{-3/2} q_n^{-1/2}\left(\frac{R_0}{R}\right)^{3/2}$$

$$\times [\hat{\Omega}_M - (4B_{11} - \hat{\Omega}_M^2)^{1/2}]\ \text{Hz}\ . \qquad (3.10)$$

Figure 5 shows $f_{\max}$ as a function of initial β for $n = 0$, 0.5, and 1. For a given β, the maximum frequency is smaller for larger n, as a result of the rotational expansion factor R/R_0. This dependence on n is significant only for larger β and $n \gtrsim 1$. For comparison, we also show in Figure 5 twice of the rotational frequency of the Maclaurin spheroid $2f_M = \Omega_M/\pi$. This would be the frequency of the gravitational wave emitted if the rapidly rotating star were deformed slightly away from axisymmetry by external stress (e.g., a mountain on the neutron star). This frequency is larger than 1000 Hz if the star rotates sufficiently rapidly to be secularly unstable.

3.3. *Characteristic Wave Amplitude*

Thorne (1987) has emphasized the importance of the signal-to-noise ratio of a given source when considering its detectability. For a broad-band detector such as LIGO, the best signal-to-noise ratio will be obtained by matched filtering of the data, $S/N \simeq h_c/h_{\rm rms}$, where $h_{\rm rms}$ is the interferometer's root mean square noise (Abramovici et al. 1992), and h_c is the characteristic amplitude of the source. For the quasi-static evolution discussed in § 3.2, h_c is given by[3]

$$h_c \equiv h\left|\frac{dN}{d\ln f}\right|^{1/2} = \frac{1}{D}\left(\frac{5}{2\pi}\left|\frac{dE}{d\Omega}\right|_{\rm eq}\right)^{1/2}$$

$$= \frac{M}{D}\left(\frac{R_0}{M}\right)^{1/4}\left(\frac{5}{2\pi}\left|\frac{d\bar{E}}{d\bar{\Omega}}\right|_{\rm eq}\right)^{1/2}, \qquad (3.11)$$

where $\bar{E} = E/(M^2/R_0)$, $\bar{\Omega} = \Omega/(M/R_0^3)^{1/2}$, and we have used equations (3.7)–(3.8).

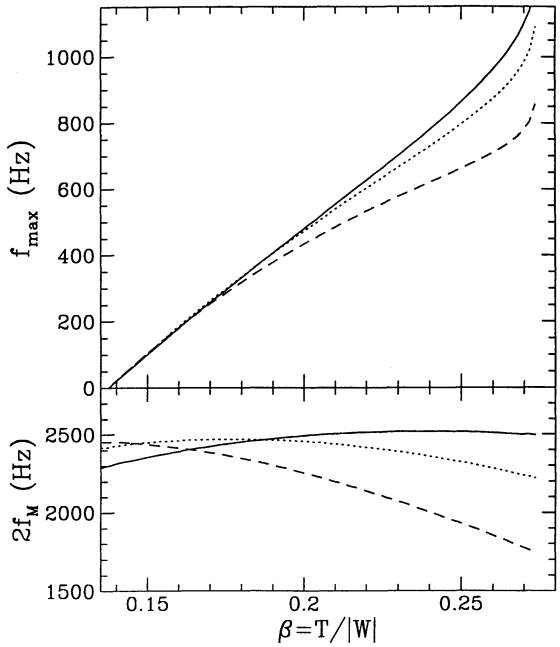

FIG. 5.—(*top*) The maximum frequency $f_{\max}$ of the gravitational wave radiated during the evolution of a neutron star from unstable Maclaurin spheroid to stable Dedekind ellipsoid as a function of the initial $T/|W|$. The solid line is for $n = 0$, the dotted line for $n = 0.5$, and the dashed line for $n = 1$. (*bottom*) Twice of the rotational frequency of the initial Maclaurin spheroid. Here $M = 1.4\,M_\odot$ and $R_0 = 10$ km.

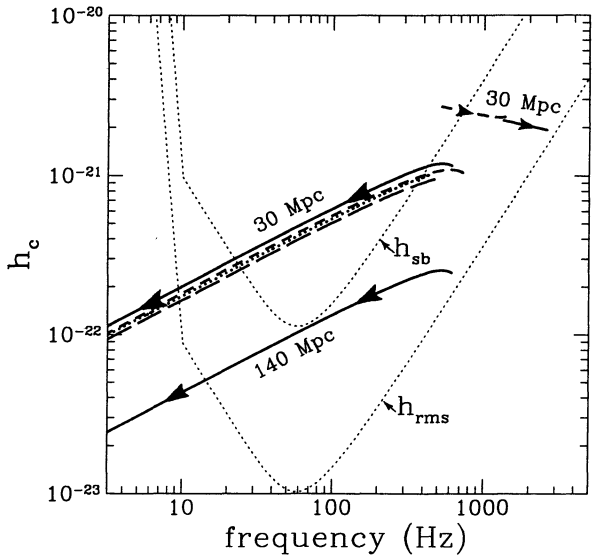

FIG. 6.—Comparison between the characteristic amplitude h_c of gravitational waves emitted during the secular evolution of a nonaxisymmetric neutron star and the rms noise $h_{\rm rms}$ in LIGO's advanced detector. The heavy lines in the center of the figure correspond to the evolution shown in Fig. 4, while those in the right upper corner correspond to the evolution shown in Fig. 7 (but here only the solid and dotted lines are shown for clarity).

In Figure 6, we show h_c for the four wave amplitudes depicted in Figure 4, and compare them with the rms noise $h_{\rm rms}$ and the sensitivity to bursts $h_{\rm sb} = 11h_{\rm rms}$ of the advanced LIGO detector (Abramovici et al. 1992). From our numerical calculations, we find $(d\bar{E}/d\bar{\Omega})_{\rm eq} \propto \bar{\Omega}$ to a good approximation. Thus the characteristic amplitude of gravitational wave during the evolution from a Maclaurin spheroid to a Dedekind Ellipsoid is given by

$$h_c \simeq 6.0 \times 10^{-23}\left(\frac{30\ \text{Mpc}}{D}\right) M_{1.4}^{3/4} R_{10}^{1/4} f^{1/2}\ , \qquad (3.12)$$

where f is the wave frequency in Hertz. This expression is accurate to within ~20% to all relevant values of β and n ($0.16 < \beta < 0.27$, $0 \le n \le 1.5$). We see clearly from Figure 6 that *the gravitational waves from the nonaxisymmetric evolution of rapidly rotating neutron stars should be detectable with high confidence* (S/N > 11) *out to the distance of* ~140 Mpc *by the advanced LIGO detector at* ~100 Hz. Valuable information about the masses and radii, as well as the rotation rates of newly formed neutron stars may be gained from the unique wave signatures (Figs. 4–5).

4. OTHER TYPES OF WAVE FORM

The low-frequency gravitational wave discussed in § 3 results from the Maclaurin-Dedekind transition (region I in

[3] More precisely, one needs to average over the source direction to obtain h_c (Thorne 1987), but this only introduces a factor $(4/5)^{1/2}$ in eq. (3.11).

Fig. 2). Apart from this low-frequency wave, there are two other types of gravitational waveforms that one may expect, at least in principle, during the evolution of a Riemann-S ellipsoid due to gravitational radiation.

4.1. "*Spin-up*" *Waves*

A Jacobi-like ellipsoid ($|\zeta| < 2|\Omega|$) will evolve to become a stable Maclaurin spheroid if $|\mathscr{C}| < |\mathscr{C}_{\rm sec}|$. If $|\mathscr{C}| > |\mathscr{C}_{\rm sec}|$, it will evolve toward a secularly unstable Maclaurin spheroid, and then, after a nonaxisymmetric perturbation, it will further evolve to become a Dedekind ellipsoid. The evolution of a Jacobi-like ellipsoid toward a Maclaurin spheroid (regions II and III in Fig. 2) is accompanied by emitting *gravitational wave with increasingly high frequency*.

A special case is the evolution of a Jacobi ellipsoid. From Figure 2, we see that a Jacobi ellipsoid will evolve toward a secularly stable Maclaurin spheroid.[4] Chandrasekhar (1970b) first noted that the rotational frequency increases as the Jacobi ellipsoid evolves under gravitational radiation. This spin-up is caused by the decrease of the momentum of inertia as the angular momentum is radiated away. However, it was assumed that the evolution is along the equilibrium Jacobi sequence. Thus the evolution ends up at the bifurcation point. This assumption is not valid since $\mathscr{C}$ is not conserved along a Jacobi sequence. The correct evolutionary sequence was computed by Miller (1974) for incompressible configurations.

Ipser & Managan (1984) also considered gravitational wave emission from the evolution of a compressible Jacobi elipsoid, based on their numerical models of rotating polytropes. They too made the assumption that the evolution is along a Jacobi sequence, terminating at the bifurcation point. Because of the mass-shedding constraint, exactly uniform rotating Jacobi ellipsoid exist only for $n \lesssim 0.8$. Even for $n = 0.5$, the initial uniformly rotating Jacobi ellipsoid is very close to the bifurcation point. Thus Ipser & Managan (1984) found that only a small fraction ($\sim 10^{-4}$–10^{-3}) of the mass energy can be radiated as gravitational wave, and the wave is nearly monochromatic with $f \simeq \Omega_{\rm sec}/\pi \sim 2300$–$2500$ Hz (see Fig. 5*b*). This may be somewhat misleading. Indeed, if slight differential rotation can inhibit the mass shedding of a Jacobi ellipsoid, as argued in § 2, a more deformed triaxial Jacobi configuration might exist in principle. As such a highly deformed Jacobi ellipsoid evolves toward a Maclaurin spheroid, much more energy can be emitted, and the frequency can span a wider range.

In Figure 7 we show the gravitational waveforms when a Jacobi-like triaxial ellipsoid evolves toward a Maclaurin spheroid for $n = 1$. The terminal Maclaurin spheroids (with the same $\mathscr{C}$ as the initial states) have $\beta = 0.02, 0.12, 0.135$, and 0.24. In the first three cases, the evolution ceases once the Maclaurin branch is reached, while in the last case, the Maclaurin spheroid (with $\beta = 0.24$) can evolve further to a Dedekind ellipsoid (see § 3). In the cases with $\beta = 0.12$ and 0.135, the initial state is chosen to be a Jacobi ellipsoid. The evolution is from low frequency to high (from left to right in Fig. 7). This is very different from the cases discussed in § 3.2 (see Fig. 4). The terminal frequency f_t is determined by the pattern speed Ω_t of the ellipsoid as it approaches a Maclaurin shape. This pattern speed is equal to the angular frequency of the rotating frame in

[4] For a more compressible configuration with $n \gtrsim 1.5$, a Jacobi ellipsoid will first evolve toward a secularly unstable Maclaurin. This dependence on compressibility comes from the expansion of the star as it gets more deformed due to rotation or internal motion. See Fig. 2 in Paper II.

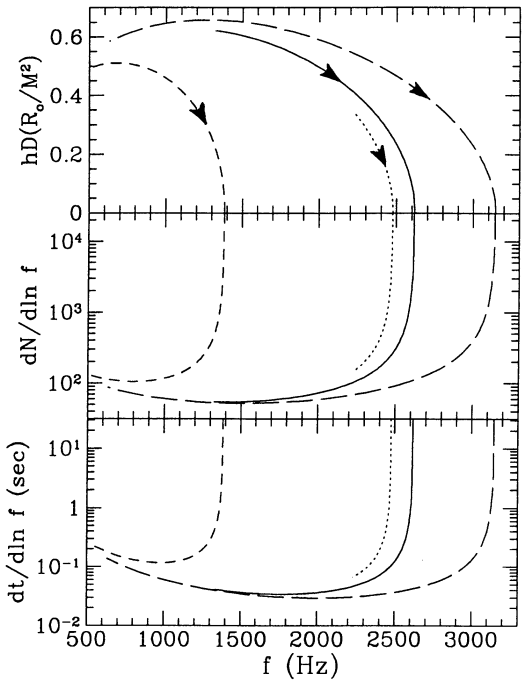

FIG. 7.—Gravitational radiation from the evolution of Jacobi-like ellipsoids (regions II and III in Fig. 2). The quantities shown are labeled as in Fig. 4. The polytropic index is $n = 1$, while $M = 1.4M_\odot$ and $R_0 = 10$ km. The solid lines and the dotted lines start from a Jacobi ellipsoid, end in a Maclaurin spheroid with $\beta = 0.12$ and $\beta = 0.135$. The short-dashed lines correspond to evolution toward a Maclaurin with $\beta = 0.24$, and the long-dashed lines to $\beta = 0.02$.

which the Jacobi mode (with minus sign in eq. [2.4]) becomes neutralized, i.e., $\sigma_-(\Omega_t) = 0$. Thus we have

$$\Omega_t = \tfrac{1}{2}(\Omega_M + \sigma_0)\,, \tag{4.1}$$

and the terminal (maximum) wave frequency is $f_t = \Omega_t/\pi$. Figure 8 depicts f_t as a function of β of the Maclaurin spheroid. Note that at the bifurcation point, we have $\Omega_t = \Omega_M = \Omega_{\rm sec}$, and at the dynamical stability limit ($\sigma_0 = 0$), we obtain $\Omega_t = \Omega_{\rm max} = \Omega_M/2$.

As seen from Figure 7 and Figure 4, the evolution of a Jacobi-like ellipsoid toward a Maclaurin spheroid is generally much faster than the evolution of a secularly unstable Maclaurin toward a Dedekind ellipsoid. This is because a typical "Jacobi-like" configuration has larger $|\Omega|$ than a typical "Dedekind-like" configuration, and because the energy radiation rate (eq. [3.5]) depends on Ω through a higher power law. For the same reasons, the typical wave amplitude during the "Jacobi-like" evolution is typically more than 10 times larger than the wave amplitude during the "Dedekind-like" evolution. However, the frequencies of the wave are much larger for the "Jacobi-like" evolution, typically $f \gtrsim 1000$ Hz.

The characteristic wave amplitude h_c during the "Jacobi-like" evolution discussed here can also be calculated using equation (3.11). These are also plotted in Figure 6. Again, h_c can be fitted to the form

$$h_c \simeq 9.1 \times 10^{-21}\left(\frac{30\ {\rm Mpc}}{D}\right) M_{1.4}^{3/4} R_{10}^{1/4} f^{-1/5}\,. \tag{4.2}$$

This expression is approximately valid for all values of $\mathscr{C}$ and n, and the differences resulting from different $\mathscr{C}$, n and initial

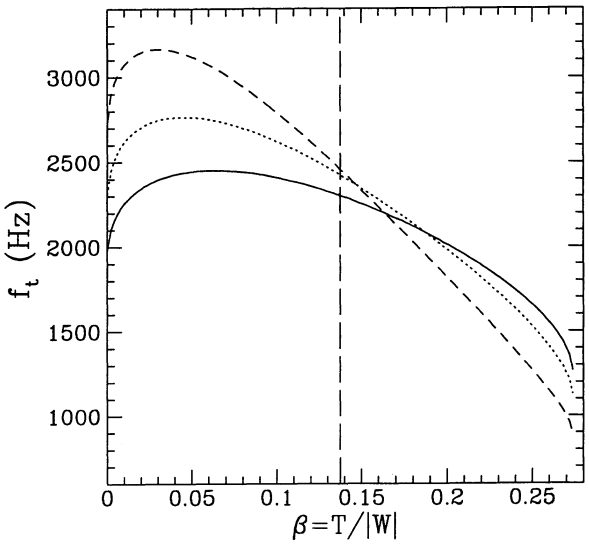

FIG. 8.—Terminal frequency of the Jacobi-like evolution as a function of $T/|W|$ of the final Maclaurin spheroid. The vertical line marks the bifurcation point.

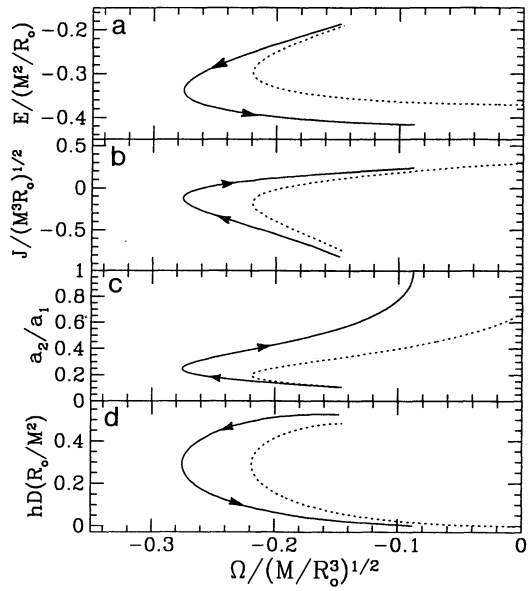

FIG. 9.—The evolution of Dedekind-like ellipsoids (corresponding to region IV in Fig. 2) emitting gravitational waves which carry negative angular momentum. (*a*) shows the equilibrium energy, (*b*) the angular momentum, (*c*) the axis ratio, and (*d*) the gravitational wave amplitude. Ω is the angular velocity of the ellipsoidal figure, so that frequency of the wave is $|\Omega|/\pi$. The solid lines correspond to $\bar{\mathscr{C}} = \mathscr{C}/M^3R_0)^{1/2} = -0.237$, the terminal configuration is a Maclaurin spheroid with $\beta = 0.1$; the dotted lines correspond to $\bar{\mathscr{C}} = -0.321$, for which the final state is a Dedekind ellipsoid with $\Omega = 0$. The polytropic index is $n = 1$.

conditions lie in the different wave frequency band. Although h_c during a "Jacobi-like" evolution is larger than h_c during a "Dedekind-like" phase, the later is actually easier to detect since the frequency lies around 100 Hz, at which LIGO detectors are most sensitive.

4.2. *Waves that Carry Negative Angular Momentum*

The third type of gravitational wave results from the evolution in region IV of Figure 2. The initial configuration is Dedekind-like ($|\zeta| > 2|\Omega|$), but with the pattern speed $\Omega < 0$, i.e., $\boldsymbol{\Omega}$ is opposite to the internal vorticity $\boldsymbol{\zeta}$ which provides major contribution to the angular momentum $\boldsymbol{J}$ of the system. Such a configuration will evolve toward a Dedekind ellipsoid (with terminal $\Omega = 0$) when $|\mathscr{C}| > |\mathscr{C}_{\rm sec}|$, or toward a stable Maclaurin spheroid (with terminal $\Omega < 0$; see eq. [3.9]) when $|\mathscr{C}| < |\mathscr{C}_{\rm sec}|$. Figure 9 depicts two examples of such evolution. Note that Ω does not change monotonically as the a_2/a_1 decreases. For an extremely large deformation (small a_2/a_1), $\boldsymbol{J}$ is in the same direction as $\boldsymbol{\Omega}$, and $|J|$ decreases and $|\Omega|$ increases during the evolution. When the deformation is not too large, the total angular momentum of the system is positive due to the large positive internal vorticity ζ. As the system evolves toward the terminal state (Dedekind or Maclaurin), *the energy decreases but the angular momentum* $|J|$ *increases, while the ellipsoid spins down* ($|\Omega|$ *decreases*). This peculiar behavior comes about because Ω is negative, and $dE = \Omega\, dJ$ must be satisfied for secular evolution via gravitational radiation dissipation (Ostriker & Gunn 1969). The gravitational wave carries away negative angular momentum, resulting in an increase of the angular momentum of the system. The wave frequency can also be low, but the wave amplitude decreases monotonically.

It is not clear whether the waveforms discussed in this section is ever relevant to a new-born neutron star. This depends on whether the collapsed core is axisymmetric or non-axisymmetric after hydrostatic equilibrium is established following the initial implosion and/or the dynamical instability. Earlier calculations by Durisen et al. (1986) and Williams & Tohline (1988) found that a dynamically unstable rotating star evolves toward a triaxial bar surrounded by a ring. Recent calculations by Houser et al. (1994), which include shock dissipation of the ejected gas, suggest that the final outcome is an axisymmetric core surround by a shocked halo. Clearly this issue will be resolved only by three-dimensional collapsing simulations, which have yet to be performed[5]. Nevertheless, the gravitational waveforms discussed in § 3.3 and in the present section represent three classes of waveforms that can be expected from the secular nonaxisymmetric evolution of any rotating star.

5. EFFECTS OF VISCOSITY

So far in our discussion we have assumed that the star consists of inviscid fluid. When the fluid viscosity is sufficiently large, it tends to counteract the GR instability (Lindblom & Detweiler 1977). From analysis in Appendix A, the combined effect of viscosity and GR reaction is determined by the ratio of the gravitational radiation timescale and the viscous timescale, $Q \sim t_{\rm GW}/t_{\rm visc}$, or, more precisely (eq. [A33])

$$Q = 4.4 \times 10^{-13}\left(1 - \frac{n}{5}\right)^2 R_{10}^2\, M_{1.4}^{-3}\, \bar{\nu}\,, \qquad (5.1)$$

where $\bar{\nu}$ is the mean kinematic shear viscosity in units of $\rm cm^2\ s^{-1}$. Figure 10 shows the critical $T/|W|$ for instability as a function of Q for a Maclaurin spheroid with $n = 0$, 0.5, 1 and 1.5. For $Q \lesssim 1$, the instability is mainly caused by GR reaction in the "Dedekind-like" mode, while for $Q \gtrsim 1$, it is mainly

[5] In the binary coalescence calculation of Rasio & Shapiro (1994), a Jacobi-like triaxial system is produced for a sufficiently small polytropic index. However, this calculation starts from a corotating binary near contact. Calculations starting from nonsynchronized spins (more realistic for neutron stars) may yield a different result; see Shibata, Nakamura, & Oohara 1992.

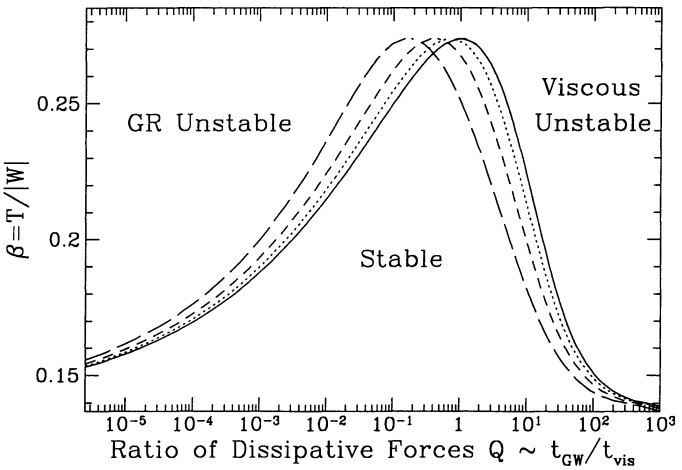

FIG. 10.—Competition of viscosity and gravitational radiation on the stability of a Maclaurin spheroid for $n = 0$ (*solid line*), $n = 0.5$ (*dotted line*), $n = 1$ (*short-dashed line*) and $n = 1.5$ (*long-dashed line*).

induced by viscous stress in the "Jacobi-like" mode. In the limits of $Q \gg 1$ and $Q \ll 1$, both instabilities set in at the bifurcation point $\beta_{sec} = 0.1375$. For $Q \sim 1$, both modes are stabilized, and the Maclaurin spheroid can be stable all the way to the dynamical limit for certain value of $Q \sim 1$.

The secular evolution discussed in § 2–4 typically occurs during the first 1–100 s after the neutron star's birth. During this epoch, the neutron star remains very hot, with temperature $T \gtrsim 10^{10}$ K (Burrows & Lattimer 1986). The shear viscosity resulting from neutron-neutron scattering is $\bar{\nu}_n \sim 10\rho_{15}^{5/4}T_{10}^{-2}$ cm^2 s^{-1} (Flowers & Itoh 1976, with the fitting formula from Cutler & Lindblom 1987), where ρ_{15} is the density in units of 10^{15} g cm^{-3}, and $T_{10} = T/(10^{10}$ K). This is much too small to have any effect on the secular instability and evolution discussed in § 2–4. The neutrino-induced shear viscosity (resulting from neutrino-neutron scattering) $\bar{\nu}_\nu \sim 10^6\rho_{15}^{-4/3}T_{10}$ cm^2 s^{-1} (Thompson & Duncan 1993) is also too small to be of any importance.

There have been some discussions about the importance of neutron star bulk viscosity in the literature. For a hot neutron star, a bulk viscosity can arise from the phase lag between density and pressure perturbation due to the relatively long timescale of weak interactions to reestablish chemical equilibrium (Sawyer 1989). In our ellipsoidal model, the bar mode is associated with the perturbations of the three axes given by $\delta a_1 = -\delta a_2$, $\delta a_3 = 0$. Therefore the bulk viscosity has no effect on the damping/growth time of the mode. In realistic calculations, however, there is a small but nonzero compression/expansion of the fluid associated with the bar mode, thus bulk viscosity can play a role (Ipser & Lindblom 1991). Using Sawyer's formula for bulk viscosity $\bar{\nu}_B \sim 10^{11}\rho_{15}T_{10}^6$ cm^2 s^{-1} (where we have taken the perturbation timescale to be of order a millisecond), Ipser & Lindblom (1991) found that the bulk viscosity can suppress the GR driven instability for $T \gtrsim 2 \times 10^{10}$ K[6]. However, it should be noted that the above formula for bulk viscosity assumes that the neutrinos produced in electron-capture escape the neutron star freely. Thus the formula is valid only for relatively low temperatures (less than a few times 10^9 K; e.g., Shapiro & Teukolsky 1983). During the early epoch of the neutron star studied in this paper, the neutrino optical depth is large, and the bulk viscosity is likely to be greatly suppressed due to the blocking of the neutrino phase space. A more detailed study is needed to fully address this issue.

In the presence of shear viscosity, the fluid circulation evolves according to

$$\frac{d\mathscr{C}}{dt} = -\bar{\nu}M\Lambda\left(\frac{a_1^2 - a_2^2}{a_1 a_2}\right)^2, \tag{5.2}$$

(cf. Paper II). This result and equation (3.5) for dJ/dt govern the secular evolution of a general ellipsoid under the combined effects of viscosity and GR reaction. Some evolutionary tracks have been considered by Detweiler & Lindblom (1977) for incompressible configurations.

Now let us consider the effect of a small viscosity on the secular evolution. Without viscosity, we see from § 3 that a Dedekind ellipsoid is one of the possible final states of the evolution. When viscosity is also present, however small, only a secularly stable Maclaurin spheroid can be the final state—it is the only configuration which does not radiate GR or dissipate energy viscously. As the star approaches a Dedekind ellipsoid, the gravitational evolution timescale increases. When this timescale becomes comparable to the viscous dissipation timescale, the star will be driven along a nearly-Dedekind sequence, eventually toward the bifurcation point. Thus we can expect that *many rapidly rotating nascent neutron stars eventually settle down at the bifurcation point along the Maclaurin sequence.* Of course, the stars can then be subjected to further spin-down due to magnetic braking.

6. DISCUSSIONS

Thorne (1987, 1992) has summarized the three radically different scenarios of rapidly rotating collapse and the resulting wave characteristics: (1) the star remains axisymmetric throughout the collapse, resulting in a weak wave signal; (2) the star becomes a (Jacobi-like) triaxial object, emitting nearly monochromatic waves with $f \sim 1000$ Hz; (3) the core breaks up into lumps, resulting in the strongest wave signal. Regarding characteristic 2, we have shown in § 4 that in general the wave emitted by a Jacobi-like rotating star can span a wide frequency band up to a few thousands Hertz. Moreover, we have considered in this paper the gravitational wave signal in another likely scenario for the post-collapse, quasi-static stage: After the hydrodynamical collapse which lasts ~ 1 s, the core settles down into a nearly axisymmetric, equilibrium state, which is secularly unstable to nonaxisymmetric perturbations. Prior to this, the star may have gone through a nonaxisymmetric dynamical phase, but the development of the dynamical instability can only render the final configuration dynamically stable and not necessarily secularly stable (Houser et al. 1994). Due to the bar-mode instability of gravitational radiation reaction (Chandrasekhar 1970a; Friedman & Schutz 1978), the nascent neutron star evolves quasi-statically toward a Dedekind-like object on a timescale of tens of seconds to a few minutes, emitting gravitational waves with frequency sweeping from a few hundred Hertz down to zero, and a nonmonotonic wave amplitude. The viscous forces finally bring the Dedekind-like neutron star to an axisymmetric Maclaurin spheroid near the bifurcation point on a much longer, viscous timescale.

[6] Ipser & Lindblom only considered uniformly rotating models and were thus restricted to rotation frequencies below the mass shedding limit.

Gravitational radiation resulting from the Chandrasekhar-Friedman-Schutz instability has been dicussed in the context of accreting neutron stars (Wagoner 1984). As a slowly rotating neutron star accretes mass from a binary companion, it can be spun up until it becomes rotationally unstable on an accretion timescale. A monochromatic gravitational wave is then radiated, carrying off the angular momentum of the accreted material. During accretion, which increases the star's angular momentum very slowly, the neutron star can evolve only slightly above the stability limit. Accordingly it is often the instability of a higher order ($m = 4$–6) mode (which sets in at smaller β) that is relevant, and the star can never reach the bar-mode ($m = 2$) stability limit (at $\beta = \beta_{\rm sec}$). Much effort has been devoted in calculating accurately the stability limits of these high-order modes (e.g., Ipser & Lindblom 1990, 1991). By contrast, in the core collapse considered in this paper, the nascent neutron star can easily reach a value of β much larger than the secular stability limit $\beta_{\rm sec}$, as a result of the much violent initial implosion. Thus in this case, the dominant instability is the bar mode. Schutz (1989) has also noted that the instability-driven spin-down can yield low frequency gravitational waves, but he has focused on the high-order modes. As we noted before, unlike the bar-mode instability, the quantitative outcome of a high-order instability is not yet clear at present.

One important question we have not addressed so far is the size R_0 of the collapsed core. The gravitational wave frequency depends sensitively on this quantity through $f \propto R_0^{-3/2}$ (cf. eq. [3.10]). We have adopted $R_0 = 10$ km throughout the paper. While the thermal pressure is unlikely to affect the radius of the collapsed core appreciably (§ 2), it is possible that the collapse can be stopped by centrifugal forces at subnuclear density. Such "centrifugal" bounce has been found in some numerical simulations of axisymmetric collapse (Mönchmeyer et al. 1991; Yamada & Sato 1993). If this indeed occurs, the wave frequency would be lower and the evolution timescale longer than discussed in this paper, although the characteristics of the waves do not change. On the other hand, it is conceivable that any realistic rotating core will ultimately contract to typical neutron star size. This must be the case if we believe that most neutron stars are born with high spin rate. Actual detection of gravitational waves from newly formed neutron stars might provide valuable information about the size and rotational properties of the collapsed cores and the dynamics of core collapse itself.

This work has been supported in part by NSF Grant AST 91-19475 and NASA Grant NAGW-2364 to Cornell University.

APPENDIX A

THE SECULAR INSTABILITY GROWTH TIMES OF COMPRESSIBLE MACLAURIN SPHEROIDS

To calculate the oscillation modes of a Maclaurin spheroid, we start from the general dynamical equations for a Riemann-S ellipsoid, including the viscous forces and gravitational radiation (GR) reaction (see Paper II, § 2, 4):[7]

$$\ddot{a}_1 = a_1(\Omega^2 + \Lambda^2) - 2a_2\Omega\Lambda - \frac{2\pi}{q_n} a_1 A_1 \bar{\rho} + \left(\frac{5k_1}{n\kappa_n}\right)\frac{P_c}{\rho_c}\frac{1}{a_1} - \frac{10}{3\kappa_n}\bar{\nu}\left(\frac{2\dot{a}_1}{a_1} - \frac{\dot{a}_2}{a_2} - \frac{\dot{a}_3}{a_3}\right)\frac{1}{a_1} - \frac{2}{5} I_{11}^{(5)} a_1 , \tag{A1}$$

$$\ddot{a}_2 = a_2(\Omega^2 + \Lambda^2) - 2a_1\Omega\Lambda - \frac{2\pi}{q_n} a_2 A_2 \bar{\rho} + \left(\frac{5k_1}{n\kappa_n}\right)\frac{P_c}{\rho_c}\frac{1}{a_2} - \frac{10}{3\kappa_n}\bar{\nu}\left(\frac{2\dot{a}_2}{a_2} - \frac{\dot{a}_1}{a_1} - \frac{\dot{a}_3}{a_3}\right)\frac{1}{a_2} - \frac{2}{5} I_{22}^{(5)} a_2 , \tag{A2}$$

$$\ddot{a}_3 = -\frac{2\pi}{q_n} a_3 a_3 \bar{\rho} + \left(\frac{5k_1}{n\kappa_n}\right)\frac{P_c}{\rho_c}\frac{1}{a_3} - \frac{10}{3\kappa_n}\bar{\nu}\left(\frac{2\dot{a}_3}{a_3} - \frac{\dot{a}_1}{a_1} - \frac{\dot{a}_2}{a_2}\right)\frac{1}{a_3} - \frac{2}{5} I_{33}^{(5)} a_3 , \tag{A3}$$

$$\frac{d}{dt}(a_1\Omega - a_2\Lambda) = -\dot{a}_1\Omega + \dot{a}_2\Lambda - \frac{5}{\kappa_n}\bar{\nu}\frac{a_1^2 - a_2^2}{a_1^2 a_2}\Lambda - \frac{2}{5} I_{12}^{(5)} a_1 , \tag{A4}$$

$$\frac{d}{dt}(-a_2\Omega + a_1\Lambda) = \dot{a}_2\Omega - \dot{a}_1\Lambda - \frac{5}{\kappa_n}\bar{\nu}\frac{a_1^2 - a_2^2}{a_1 a_2^2}\Lambda - \frac{2}{5} I_{12}^{(5)} a_2 , \tag{A5}$$

The dynamical variables are the three axes a_i ($i = 1, 2, 3$), the angular frequency of the figure (pattern speed) Ω, and the angular frequency Λ specifying the internal fluid motion (relative to the figure) with uniform vorticity $\zeta = -[(a_1^2 + a_2^2)/a_1 a_2]\Lambda$. The other quantities have the same meaning as in Paper II.

When linearizing the dynamical equations, we must allow for the fact that a Maclaurin spheroid need not be assigned the angular frequency of the frame in which it is at rest. When viewed from a rotating frame with angular frequency Ω relative to the inertial frame, the Maclaurin spheroid will appear as having stationary internal motion with the uniform vorticity $\zeta = 2(\Omega_{\rm M} - \Omega)$, i.e., $\Lambda = \Omega - \Omega_{\rm M}$, where $\Omega_{\rm M}$ is the angular frequency of the Maclaurin spheroid relative to an inertial frame. Thus the values of $\Omega_{\rm eq}$ and $\Lambda_{\rm eq}$ for the equilibrium Maclaurin spheroid can in principle be arbitrary, subject only to the condition

$$\Omega_{\rm eq} - \Lambda_{\rm eq} = \Omega_{\rm M} . \tag{A6}$$

[7] A bulk viscosity contribution, which was not included in Paper II, can be easily incorporated by adding a term $-(5\bar{\nu}_B/\kappa_n)(\dot{a}_1/a_1 + \dot{a}_2/a_2 + \dot{a}_3/a_3)/a_1$ to the right-hand side of equation (A1) and similar terms to equations (A2)–(A3), where $\bar{\nu}_B$ is the mean kinematic bulk viscosity. However, this will have no effect on the bar mode in which we are most interested here.

Consider small perturbations of the form

$$a_i = a_{i,\mathrm{eq}}(1 + \alpha_i)\,, \qquad \Omega = \Omega_{\mathrm{eq}} + \omega\,, \qquad \Lambda = \Lambda_{\mathrm{eq}} + \lambda\,, \tag{A7}$$

with $\alpha_i \propto e^{-i\sigma t}$ and similarly for ω, λ. Note that Ω_{eq} (or Λ_{eq}) must be determined from the linear mode analysis. We are only interested in the nonaxisymmetric bar mode (called "toroidal mode" in Ch69) for which it turns out $\alpha_1 = -\alpha_2$ and $\alpha_3 = 0$ (see Paper II, § 3.3).

A1. PURE DYNAMICAL OSCILLATIONS

First consider the case when viscosity and GR reaction are absent. A useful expression is

$$\frac{a_j}{A_i}\frac{\partial A_i}{\partial a_j} = \begin{cases} -2 + 3B_{ii}/A_i\,, & \text{if } i = j\,; \\ B_{ij}/A_i\,, & \text{if } i \neq j\,, \end{cases} \tag{A8}$$

(no summation for repeated indices), where A_i, B_{ij} are defined as in Ch69 (chap. 3). Also it is useful to note that the pressure term in equations (A1)–(A3) can be written as $5k_1P_c/(n\kappa_n\rho_c) = (M/q_nR_0)(R_0/R)^{3/n} = 5U/(n\kappa_n M)$, where U is the internal energy (Paper II, eq. [2.9]). Linearizing equation (A1) and using the equilibrium conditions (Paper II, eq. [3.24]), we obtain

$$\begin{aligned} I_{11}\ddot{\alpha}_1 = {} & I_{11}[\Omega_M^2\alpha_1 + 2\Omega_{\mathrm{eq}}\Lambda_{\mathrm{eq}}(\alpha_1 - \alpha_2) + 2\Omega_{\mathrm{M}}(\omega - \lambda)] + \Sigma a_1^2[(3B_{11} - 2A_1)\alpha_1 + (B_{11} - A_1)\alpha_2 + (B_{13} - A_1)\alpha_3] \\ & - \Sigma a_3^2 A_3[-\alpha_1 - (\alpha_1 + \alpha_2 + \alpha_3)/n]\,, \end{aligned} \tag{A9}$$

where the notation is the same as in Paper II (§ 3.3), with $I_{11} = \kappa_n M a_1^2/5$ and $\Sigma \equiv -3M^2/[2(5-n)R^3]$. The equation for $\ddot{\alpha}_2$ can be obtained by inter-changing subscript 1 and 2 in (A9). Linearizing equations (A4)–(A5) yields

$$\Omega_{\mathrm{eq}} = -\Lambda_{\mathrm{eq}} = \frac{\Omega_{\mathrm{M}}}{2}\,, \tag{A10}$$

$$\omega - \lambda = -\Omega_{\mathrm{M}}(\alpha_1 + \alpha_2)\,, \tag{A11}$$

where we have used $\Omega_{\mathrm{eq}} - \Lambda_{\mathrm{eq}} = \Omega_{\mathrm{M}}$ (eq. [A6]). Substituting (A10)–(A11) into (A9) and the corresponding equation for $\ddot{\alpha}_2$, we can see that $\alpha_1 = -\alpha_2$, $\alpha_3 = 0$ is indeed a solution. After some algebra, we obtain

$$I_{11}\Delta\ddot{\alpha} = -I_{11}\sigma_0^2\Delta\alpha\,, \tag{A12}$$

where $\Delta\alpha \equiv \alpha_1 - \alpha_2$, and

$$\sigma_0 = \left(\frac{4}{q_n}\pi\bar{\rho}B_{11} - \Omega_{\mathrm{M}}^2\right)^{1/2}. \tag{A13}$$

Thus the mode frequency is $\sigma = \pm\sigma_0$, in agreement with the result of Paper II, obtained using a Hamiltonian formalism. Note that the frequency σ_0 is viewed in a particular rotating frame with $\Omega = \Omega_{\mathrm{M}}/2$, in which the oscillation is self-adjointed ($\Omega = -\Lambda$), and the directions of the principal axes of the ellipsoid are fixed (Ch69, § 36). In a frame with a different Ω, the oscillation frequency is

$$\sigma_\pm(\Omega) = \pm\sigma_0 + 2\left(\Omega - \frac{\Omega_{\mathrm{M}}}{2}\right), \tag{A14}$$

since this corresponds to a $l = m = 2$ mode with a exp $(i2\phi)$ dependence on the azimuthal angle (see Ch69, § 36; Rossner 1967).

A2. EFFECT OF VISCOSITY

Now consider a small viscosity $\bar{\nu}$ so that we only consider the leading correction $\sim\mathcal{O}(\bar{\nu})$ to the mode frequency. Again assuming a $e^{-i\sigma t}$ time dependence of the perturbations, from equations (A4)–(A6) we obtain

$$\Omega_{\mathrm{eq}} = \frac{1}{2}\Omega_{\mathrm{M}}\left(1 + i\frac{5\bar{\nu}}{\kappa_n a_1^2\sigma}\right), \qquad \Lambda_{\mathrm{eq}} = -\frac{1}{2}\Omega_{\mathrm{M}}\left(1 - i\frac{5\bar{\nu}}{\kappa_n a_1^2\sigma}\right), \tag{A15}$$

while equation (A11) still holds. The fact that Ω_{eq} contains an imaginary part implies that the rotation of the frame in which the oscillation is specified can itself enhance or damp the oscillation amplitude. Substituting equations (A11) and (A15) into the linearized equations for $\ddot{\alpha}_i$, we obtain

$$\Delta\ddot{\alpha} = -\sigma_0^2\Delta\alpha - \frac{10\bar{\nu}}{\kappa_n a_1^2}\Delta\dot{\alpha}\,, \tag{A16}$$

from which we have

$$\sigma = \pm\sigma_0 - i\frac{5\bar{\nu}}{\kappa_n a_1^2}\,. \tag{A17}$$

However, this is the frequency of oscillation in a frame with angular frequency given by a complex Ω_{eq}. Similar to equation (A14), in a general frame with (real) angular velocity Ω, the oscillation frequency is

$$\sigma_{\pm}(\Omega) = \pm\sigma_0 - i\frac{5\bar{\nu}}{\kappa_n a_1^2} + 2\left[\Omega - \left(\frac{\Omega_M}{2} \pm i\frac{5\bar{\nu}\Omega_M}{2\kappa_n a_1^2\sigma_0}\right)\right] = \pm\sigma_0 + 2\left(\Omega - \frac{\Omega_M}{2}\right) - i\frac{5\bar{\nu}}{\kappa_n a_1^2}\frac{\sigma_0 \pm \Omega_M}{\sigma_0}. \tag{A18}$$

Clearly, the Dedekind mode (with upper sign in eq. [A18]) is always secularly stable. For the Jacobi mode (with lower sign in eq. [A18]), secular instability sets in when $\Omega_M > \sigma_0$, or when

$$q_n\frac{\Omega_M^2}{\pi\bar{\rho}} > 2B_{11}, \tag{A19}$$

corresponding to bifurcation values $e = 0.8127$ and $T/|W| = 0.1375$. The instability growth time τ_{vis} is given by

$$\tau_{vis}^{-1} = \frac{5\bar{\nu}}{\kappa_n a_1^2}\left(\frac{\Omega_M - \sigma_0}{\sigma_0}\right). \tag{A20}$$

A3. EFFECT OF GRAVITATIONAL RADIATION

Now to include the GR reaction, we first need to calculate $I_{ij}^{(5)}$, the fifth time derivative of the reduced quadrupole moment tensor of the body in the inertial frame projected onto the rotating body frame (with basis vectors along the principal axes). This is done using the procedure given in Miller (1974) and Appendix A of Paper II. Unlike the quasi-static case (as in Appendix A of Paper II), in order to discern the instability, $I_{ij}^{(5)}$ need to be calculated to all order. For small perturbations around a Maclaurin spheroid, we obtain

$$\begin{aligned}[I_{ij}^{(5)}] = {} & [15\Omega^5(I_{11} - I_{22}) - 40\Omega^3(I_{11}^{(2)} - I_{22}^{(2)}) + 5\Omega(I_{11}^{(4)} - I_{22}^{(4)})]\begin{pmatrix}0 & 1 & 0\\ 1 & 0 & 0\\ 0 & 0 & 0\end{pmatrix} \\ & + [40\Omega^4(I_{11}^{(1)} - I_{22}^{(1)}) - 20\Omega^2(I_{11}^{(3)} - I_{22}^{(3)})]\begin{pmatrix}1 & 0 & 0\\ 0 & -1 & 0\\ 0 & 0 & 0\end{pmatrix} \\ & + \begin{pmatrix}I_{11}^{(5)} & 0 & 0\\ 0 & I_{22}^{(5)} & 0\\ 0 & 0 & I_{33}^{(5)}\end{pmatrix},\end{aligned} \tag{A21}$$

where on the right-hand side, the superscript i now means ith time derivative in the frame of the body. Thus the only nontrivial components are therefore

$$\begin{aligned} I_{11}^{(5)} &= -\frac{40}{5}i\kappa_n Ma_1^2(\alpha_1 - \alpha_2)(2\Omega^4\sigma + \Omega^2\sigma^3) - \frac{2}{5}i\kappa_n Ma_1^2\sigma^5\alpha_1 - \frac{1}{3}I_t^{(5)}, \\ I_{22}^{(5)} &= +\frac{40}{5}i\kappa_n Ma_1^2(\alpha_1 - \alpha_2)(2\Omega^4\sigma + \Omega^2\sigma^3) - \frac{2}{5}i\kappa_n Ma_1^2\sigma^5\alpha_2 - \frac{1}{3}I_t^{(5)}, \\ I_{33}^{(5)} &= -\frac{2}{5}i\kappa_n Ma_3^2\sigma^5\alpha_3 - \frac{1}{3}I_t^{(5)}, \\ I_{12}^{(5)} &= I_{21}^{(5)} = \frac{2}{5}\kappa_n Ma_1^2(\alpha_1 - \alpha_2)(16\Omega^5 + 40\Omega^3\sigma^2 + 5\Omega\sigma^4), \end{aligned} \tag{A22}$$

where $I_t \equiv I_{11} + I_{22} + I_{33} = \kappa_n M(a_1^2 + a_2^2 + a_3^2)/5$.

Linearizing equations (A4)–(A5) including GR reaction alone, we have

$$\Omega_{eq} = \frac{1}{2}\Omega_M - i\frac{2\kappa_n Ma_1^2}{25}\frac{1}{\sigma}(16\Omega_{eq}^5 + 40\Omega_{eq}^3\sigma^2 + 5\Omega_{eq}\sigma^4) \simeq \frac{1}{2}\Omega_M - i\frac{\kappa_n Ma_1^2}{25}\frac{1}{\sigma}(\Omega_M^5 + 10\Omega_M^3\sigma^2 + 5\Omega_M\sigma^4) \tag{A23}$$

and $\Lambda_{eq} = \Omega_{eq} - \Omega_M$, where we have assumed that the GR reaction is a small correction. Linearizing equations for $\ddot{a}_i$, we obtain, for the bar mode

$$\Delta\ddot{\alpha} = -\sigma_0^2\Delta\alpha - \tfrac{2}{5}(I_{11}^{(5)} - I_{22}^{(5)}) = -\sigma_0^2\Delta\alpha + i\frac{4\kappa_n Ma_1^2}{25}[40(2\Omega_{eq}^4\sigma + \Omega_{eq}^2\sigma^3) + \sigma^5]\Delta\alpha. \tag{A24}$$

With equation (A23), we then have

$$\sigma = \pm\sigma_0 - i\frac{2\kappa_n Ma_1^2}{25}[5(\Omega_M^4 + 2\Omega_M^2\sigma_0^2) + \sigma_0^4]. \tag{A25}$$

Again, this is only the frequency of oscillation in a frame with the complex angular frequency $\Omega_{\rm eq}$. The existence of an imaginary part in $\Omega_{\rm eq}$ implies additional mode damping or growing. Similar to equation (A14), in a general frame with (real) angular velocity Ω, the oscillation frequency is

$$\sigma_{\pm}(\Omega) = \pm\sigma_0 - i\frac{2\kappa_n M a_1^2}{25}[5(\Omega_{\rm M}^4 + 2\Omega_{\rm M}^2\sigma_0^2) + \sigma_0^4] + 2(\Omega - \Omega_{\rm eq}) = \pm\sigma_0 + 2\left(\Omega - \frac{\Omega_{\rm M}}{2}\right) - i\frac{2\kappa_n M a_1^2}{25}\frac{(\sigma_0 \mp \Omega_{\rm M})^5}{\sigma_0}. \quad \text{(A26)}$$

Clearly, the Dedekind-mode become secularly unstable when equation (A19) is satisfied, i.e., the gravitational radiation also induces an instability at the bifurcation point, but for a different mode as for viscosity. The growth time $\tau_{\rm GW}$ is given by

$$\tau_{\rm GW}^{-1} = \frac{2\kappa_n M a_1^2}{25}\frac{(\Omega_{\rm M} - \sigma_0)^5}{\sigma_0}. \quad \text{(A27)}$$

A4. COMBINED EFFECTS OF VISCOSITY AND GRAVITATIONAL RADIATION

The secular bar-mode instability tends to weaken or diminish when both viscosity and GR reaction are present. This is because viscous dissipation and GR reaction cause different modes to become unstable, as seen from §§ A2 and A3. The combined effects of viscosity and GR reaction on the secular instability of incompressible Maclaurin spheroid were first noted by Lindblom & Detweiler (1977). Combining the results of §§ A2 and A3, we find that the (complex) frequency for the bar mode in a rotating frame with angular velocity Ω is given by

$$\sigma_{\pm}(\Omega) = \pm\sigma_0 + (2\Omega - \Omega_{\rm M}) - i\left[\frac{5\bar{\nu}}{\kappa_n a_1^2}\frac{\sigma_0 \pm \Omega_{\rm M}}{\sigma_0} + \frac{2\kappa_n M a_1^2}{25}\frac{(\sigma_0 \mp \Omega_{\rm M})^5}{\sigma_0}\right]. \quad \text{(A28)}$$

For convenience, let us define dimensional viscous time constant and gravitational radiation time constant via

$$t_{\rm vis}^{-1} = \frac{5\bar{\nu}}{\kappa_n R_0^2}, \qquad t_{\rm GW}^{-1} = \frac{9\kappa_n}{200 q_n^2}\left(\frac{GM}{R_0 c^2}\right)^{5/2}\left(\frac{GM}{R_0^3}\right)^{1/2}, \quad \text{(A29)}$$

(G, c have been restored). The growth time $\tau_{\pm} > 0$ of the two modes are then given by

$$\tau_+^{-1} = t_{\rm GW}^{-1}\left[(1-e^2)^{-1/3}\left(\frac{R_0}{R}\right)^4\frac{(\hat{\Omega}_{\rm M} - \hat{\sigma}_0)^5}{\hat{\sigma}_0}\right] - t_{\rm vis}^{-1}\left[(1-e^2)^{1/3}\left(\frac{R_0}{R}\right)^2\frac{\hat{\Omega}_{\rm M} + \hat{\sigma}_0}{\hat{\sigma}_0}\right], \quad \text{(A30)}$$

and

$$\tau_-^{-1} = t_{\rm vis}^{-1}\left[(1-e^2)^{1/3}\left(\frac{R_0}{R}\right)^2\frac{\hat{\Omega}_{\rm M} - \hat{\sigma}_0}{\hat{\sigma}_0}\right] - t_{\rm GW}^{-1}\left[(1-e^2)^{-1/3}\left(\frac{R_0}{R}\right)^4\frac{(\hat{\Omega}_{\rm M} + \hat{\sigma}_0)^5}{\hat{\sigma}_0}\right], \quad \text{(A31)}$$

where the quantities in square brackets are dimensionless and depend only on the eccentricity e (for compressible systems, there is also a dependence on n through R_0/R), and

$$\hat{\Omega}_{\rm M} = \frac{\Omega_{\rm M}}{\sqrt{\pi\bar{\rho}}}q_n^{1/2}, \qquad \hat{\sigma}_0 = \frac{\sigma_0}{\sqrt{\pi\bar{\rho}}}q_n^{1/2} = (4B_{11} - \hat{\Omega}_{\rm M}^2)^{1/2}. \quad \text{(A32)}$$

When $\tau_{\pm} < 0$, the mode involved is stable, and $|\tau_{\pm}|$ then gives the corresponding damping time. In the limit of $n = 0$, the above results agree with that of Lindblom & Detweiler (1977).

It is clear from the above expressions that the bar mode of a compressible Maclaurin spheroid tends to be stabilized by the combined effects of viscosity and GR reaction. To locate the region of stability, define

$$Q \equiv \frac{t_{\rm GW}}{t_{\rm vis}}(1 - e_d^2)^{2/3}\hat{\Omega}_d^{-4}, \quad \text{(A33)}$$

where $e_d = 0.95289$ and $\hat{\Omega}_d^2 = q_n\Omega_d^2/(\pi\bar{\rho}) = 0.44022$ refer to the dynamical stability limit. The Dedekind mode is stable when

$$Q\hat{\Omega}_d^4\left(\frac{1-e^2}{1-e_d^2}\right)^{2/3}\left(\frac{R}{R_0}\right)^2(\hat{\Omega}_{\rm M} + \hat{\sigma}_0) \geq (\hat{\Omega}_{\rm M} - \hat{\sigma}_0)^5, \quad \text{(A34)}$$

and the Jacobi mode is stable when

$$Q\hat{\Omega}_d^4\left(\frac{1-e^2}{1-e_d^2}\right)^{2/3}\left(\frac{R}{R_0}\right)^2(\hat{\Omega}_{\rm M} - \hat{\sigma}_0) \leq (\hat{\Omega}_{\rm M} + \hat{\sigma}_0)^5. \quad \text{(A35)}$$

Figure 10 depicts the critical $T/|W|$ (where the secular instability first sets in) as a function of Q for $n = 0, 0.5, 1, 1.5$. For $n = 0$ and $Q = 1$, the Maclaurin spheroid is stable all the way to the dynamical limit.

REFERENCES

Abramovici, A., et al. 1992, Science, 256, 325
Bahcall, J. A., & Piran, T. 1983, ApJ, 267, L77
Bailyn, C. D., & Grindlay, J. E. 1990, ApJ, 353, 159
Blair, D. 1989, in Gravitational Wave Data Analysis, ed. B. F. Schutz (Dordrecht: Kluwer)
Bodenheimer, P., & Ostriker, J. P. 1973, ApJ, 180, 159
Bonazzola, S., & Marck, J. A. 1993, A&A, 267, 623
Bradaschia, C., et al. 1990, Nucl. Instrum. Methods, A, 289, 518
Burrows, A. 1990, in Supernovae, ed. A. G. Petschek (New York: Springer), 143
Burrows, A., & Lattimer, J. M. 1986, ApJ, 307, 178
Chandrasekhar, S. 1969, Ellipsoidal Figures of Equilibrium (New Haven: Yale Univ. Press) (Ch69)
———. 1970a, ApJ, 161, 561
———. 1970b, ApJ, 161, 571
Comins, N. 1979a, MNRAS, 189, 233
———. 1979b, MNRAS, 189, 255
Cordes, J. M., Romani, R. W., & Lundgren, S. C. 1993, Nature, 362, 133
Cropper, M., et al. 1988, MNRAS, 231, 695
Cutler, C., & Lindblom, L 1987, ApJ, 314, 234
Detweiler, S. L., & Lindblom, L. 1977, ApJ, 213, 193
Durisen, R. H., Gingold, R. A., Tohline, J. E., & Boss, A. P. 1986, ApJ, 305, 281
Finn, L. S. 1991, in Ann. NY Acad. Sci. Vol. 631, Nonlinear Problems in Relativity and Cosmology, ed. J. R. Buchler, S. L. Detweiler, & J. R. Ipser, 56
Flowers, E., & Itoh, N. 1976, ApJ, 206, 218
Friedman, J., & Schutz, B. F. 1978, ApJ, 222, 281
Houser, J. L., Centrella, J. M., & Smith, S. C. 1994, Phys. Rev. Lett., 72, 1314
Imamura, J. N., Friedman, J. L., & Durisen, R. H. 1985, ApJ, 294, 474
Ipser, J. R., & Lindblom, L. 1990, ApJ, 355, 226
———. 1991, ApJ, 373, 213
Ipser, J. R., & Managan, R. A. 1984, ApJ, 282, 287
James, R. A. 1964, ApJ, 140, 552
Lai, D., Rasio, F. A., & Shapiro, S. L. 1993, ApJS, 88, 205 (Paper I)
———. 1994, ApJ, 437, 742
Lindblom, L., & Detweiler, S. 1977, ApJ, 211, 565
Managan, R. A. 1985, ApJ, 294, 463
Michel, F. C. 1987, Nature, 329, 310
Miller, B. D. 1974, ApJ, 187, 609
Misner, C. M., Thorne, K. S., & Wheeler, J. A. 1970, Gravitation (New York: Freeman)
Mönchmeyer, R., Schäfer, G., Müller, E., & Kates, R. E. 1991, A&A, 246, 417
Ostriker, J. P., & Bodenheimer, P. 1973, ApJ, 180, 171
Ostriker, J. P., & Gunn, J. E. 1969, ApJ, 157, 1395
Radhakrishnan, V. 1992, in X-Ray Binaries and Recycled Pulsars, ed. E. P. J. van den Heuvel & S. A. Rappaport (Dordrecht: Kluwer),
Rasio, F. A., & Shapiro, S. L. 1994, ApJ, 432, 242
Roberts, P. H., & Stewartson, K. 1963, ApJ, 137, 777
Rossner, L. F. 1967, ApJ, 149, 145
Saenz, R. A., & Shapiro, S. L. 1981, ApJ, 244, 1033
Sawyer, R. F. 1989, Phys. Rev. D, 39, 3804
Schutz, B. F. 1989, Class. Quantum Grav., 6, 1761
Shapiro, S. L., & Teukolsky, S. A. 1983, Black Holes, White Dwarfs, and Neutron Stars (New York: Wiley)
Shibata, M., Nakamura, T., & Oohara, K. 1992, Prog. Theor. Phys., 88, 1079
Spyromilio, J. 1994, MNRAS, 266, L61
Tassoul, J.-L. 1978, Theory of Rotating Stars (Princeton: Princeton Univ. Press)
Thompson, C., & Duncan, R. C. 1993, ApJ, 408, 194
Thorne, K. S. 1987, in 300 Years of Gravitation, ed. S. W. Hawking & W. Israel (Cambridge: Cambridge Univ. Press)
———. in Recent Advances in General Relativity, ed. A. I. Janis & J. R. Porter (Birkhauser: Boston)
Trammell, S. R., Hines, D. C., & Wheeler, J. C. 1993, ApJ, 414, L21
van den Burgh, S., & Tammann, G. A. 1991, ARA&A, 29, 363
van den Heuvel, E. P. J. 1987, in IAU Symp. 125, The Origin and Evolution of Neutron Stars, ed. D. Helfand & J. Huang (Dordrecht: Reidel), 393
Wagoner, R. 1984, ApJ, 278, 345
Williams, H., & Tohline, J. E. 1988, ApJ, 334, 449
Yamada, S., & Sato, K. 1993, preprint UTAP-154/93